

# Lawrence Berkeley National Laboratory

## Recent Work

### Title

Simulating Space Radiation-Induced Breast Tumor Incidence Using Automata

### Permalink

<https://escholarship.org/uc/item/5j9162v3>

### Authors

Heuskin, A. C.

Osseiran, A. I.

Tang, J.

et al.

### Publication Date

2016-06-22

1 **Simulating Space Radiation-Induced Breast Tumor Incidence Using Automata**

2 A.C. Heuskin<sup>1,2</sup>, A.I. Osseiran<sup>1</sup>, J. Tang<sup>3</sup> and S.V. Costes<sup>1\*</sup>

3 <sup>1</sup>Life Sciences Division, Lawrence Berkeley National Laboratory, Berkeley, CA, USA

4 Exogen Biotechnology Inc., Berkeley, CA, USA

5 <sup>2</sup> NAMur Research Institute for Life Sciences (NARILIS), Research Center for the Physics of Matter and

6 Radiation (PMR), University of Namur, Namur, Belgium

7

8

9 Running title: Automata-based space radiation risk

10

---

\* To whom the correspondence should be addressed: S.V. Costes ([svcostes@lbl.gov](mailto:svcostes@lbl.gov)), Life Sciences Division, Lawrence Berkeley National Laboratory, 1 Cyclotron Road, MS: 977, Berkeley, CA 94720, USA. Tel: (510) 486-6988/6624, Fax: (510) 486-7542.

11 **Abstract:**

12 Heuskin A.C., Osseiran A., Tang J. and Costes S.V., Simulating Space Radiation-Induced Breast Tumor  
13 Incidence Using Automata, *Radiat. Res.*

14 Estimating cancer risk from space radiation has been an ongoing challenge for decades primarily  
15 because most epidemiological data showing evidence of cancer risk from ionizing radiation are derived  
16 from studies of atomic bomb survivors, where individuals were exposed to acute dose of gamma-rays  
17 instead of chronic exposure of high-LET cosmic radiation. In this work, we introduce a formalism using  
18 cellular automata to model the long-term effects of ionizing radiation in human breast for different  
19 radiation quality. We first validate and tune parameters for an automata-based two stage clonal  
20 expansion model which simulates the age dependence of spontaneous breast cancer incidence in  
21 unexposed US population. We then test the impact of radiation perturbation in the model by modifying  
22 parameters to reflect both targeted and non-targeted effects of ionizing radiation.

23 Targeted effects (TE) reflect the immediate impact of radiation on cell's DNA with classic endpoints  
24 being gene mutations and cell death. They are well known and are directly derived from experimental  
25 data. In contrast, non-targeted effects (NTE) are persistent radiation effects affecting both damaged and  
26 undamaged cells, they are non-linear with dose and they are not well characterized in the literature. TE  
27 is first introduced in the model and predictions are compared to epidemiologic data of the A-bomb  
28 cohort. TE alone is not sufficient to induce enough cancer and genomic instability which last ~100 days  
29 post-exposure independently of dose needs to be added to predict accurately the dose dependence of  
30 breast cancer induced by gamma-rays. Finally, by integrating experimental RBE for TE and keeping  
31 radiation-induced genomic instability constant with dose and LET, the model predicts that RBE for breast  
32 cancer induced by cosmic radiation would be maximum at 220 keV/ $\mu\text{m}$ . This work is well suited to  
33 explore next the impact of chronic low dose exposure, inter-individual variation and more complex  
34 space radiation scenarii.

## 35 **1. Introduction**

36 Space programs are currently shifting to planetary exploration, in particular missions to the moon and  
37 Mars. However, the continuous exposure of astronauts to Galactic Cosmic Rays (GCR) is one of the main  
38 concerns for long term missions because of increased risk of cancer and other degenerative diseases.  
39 The GCR spectra contains a large component of high-LET particles, such as He ions and heavier ions such  
40 as carbon and iron (HZE particles, i.e. particles with high charge and energy) (1). Despite the low  
41 frequency of GCR, they are a major contributor to cancer risk because of their high ionization density  
42 which can lead to severe mutational events. High-LET ionizing radiation have been shown to induce  
43 relative biological effectiveness (RBE) as high as 40 in animal models (2). Also of concern are solar  
44 particle events (SPE) (3) whose unpredictable nature and high doses pose a risk for out-of-spacecraft  
45 tasks.

46 Unfortunately, estimating cancer risk from space radiation remains a challenge primarily because most  
47 epidemiological data showing evidence of cancer risk from ionizing radiation are derived from studies of  
48 atomic bomb survivors (4). Classic risk models rely on scaling variables, such as radiation-quality factor  
49 Q, RBE and dose and dose-rate effectiveness factors, extrapolating risk from gamma radiation (main  
50 radiation in A-bomb blast) to high-LET radiation in space.

51 This poses the question of whether risk estimates derived from sparsely ionizing radiation can be used  
52 to assess risks associated with HZE. In this work, we introduce a formalism using cellular automata, to  
53 test mechanisms that can reproduce cancer incidence, by modeling the short-term and long-term  
54 effects of ionizing radiation in tissue. Cellular automata are stochastic models where each cell is  
55 represented by an algorithmic entity with basic individual properties representing the variety of cellular  
56 behaviors (5, 6). We first establish a relationship between the dose from gamma-radiation and cell  
57 death, cell senescence, and genomic instability for various time scale. This relationship is tuned so that

58 we can predict accurately breast cancer incidence in humans (A-bomb cohort vs unexposed population).  
 59 In a second phase, the model is used to test new mechanisms of DNA misrepair and cell death from  
 60 high-LET (7) to predict high-LET response and RBE for various cosmic radiation. This model is a first step  
 61 for the growing demand of a deeper knowledge of biological processes underlying carcinogenesis and  
 62 their disruption by heavy ions (1).

## 63 2. Material and methods

### 64 2.1 Multistage expansion model: theoretical considerations

65 We focused on the concept of the multistage expansion model which provides an analytical solution to  
 66 epidemiological cancer incidence (8). This model assumes that malignant tumors arise from a series of  
 67 modifications of a single progenitor cell and that cancer is the last of a series of  $k$  sudden and  
 68 irreversible changes. For a cell which has already experienced  $(i-1)$  changes, the event rate for the next  
 69 change is  $\mu_i$ . The exact solution can be derived from Bateman's solution of successive radioactive decays  
 70 and the stage  $p_{m-1}(t)$  can be expressed as:

$$71 \quad p_{m-1}(t) = c_m \sum_{j=1}^m X_{j,m} e^{-\mu_j t} \quad (1)$$

72

73 with  $c_m = \alpha \prod_{j=1}^{m-1} \mu_{j-1,j}$  and  $X_{j,m} = \prod_{\substack{l=1 \dots m \\ l \neq j}} (\mu_l - \mu_j)^{-1}$ . The hazard rate is then  $h(t) = N \mu_k p_{k-1}(t)$

74 with  $N$  as the total number of affected cells. The first non-vanishing term in a Taylor serie of  $p_{k-1}(t)$  gives  
 75 the well-known Armitage-Doll model (9):

$$76 \quad h(t) = at^{k-1} \text{ with } a = \frac{\prod_{j=1}^k \mu_j}{(k-1)!}. \quad (2)$$

77 However this simpler model gives a power law for the age-dependent incidence and it is known that the  
 78 cancer incidence flattens above age 60 and falls below the predicted curve. Pompei and Wilson  
 79 proposed a modified version of this model by adding a senescence factor and assuming that malignant  
 80 cells are mortal in the sense of Hayflick (i.e. cell divisions are not infinite) (10). If a malignant cell is  
 81 completely senescent, this cell does not produce observable cancer. The hazard function better fits the  
 82 epidemiological data at high age (11) and takes the following form:

$$83 \quad h(t) = at^{k-1}(1 - \beta t). \quad (3)$$

84 However not all the initiated cells can progress to cancer as some of them can be repaired or removed.  
 85 This lead to a more refined model involving only two stages (k=0,1,2) and a death rate for intermediate  
 86 cells (12, 13). The Moolgavkar, Venzon and Knudson (MVK) model or two stage clonal expansion (TSCE)  
 87 model gives then a hazard of the form:

$$88 \quad h(t) = \frac{X_m(e^{(\gamma+2q)t}-1)}{q(e^{(\gamma+2q)t}+1)+\gamma} \quad (4)$$

89 where  $X_m$ ,  $\gamma$  and  $q$  can be related to actual biological parameters using the following transformations:

90  $X_m = \mu_2 v$ ;  $\gamma = \alpha - \beta - \mu_2$ ;  $q = \frac{\mu_2}{1-A}$  with  $A = \frac{b+\sqrt{b^2-4\alpha\beta}}{2\alpha}$  and  $b = \alpha + \beta + \mu_2$ . Here  $v$  is the  
 91 proportion of healthy cells that will acquire a first mutation,  $\mu_2$  is the rate of the second mutation,  $\alpha$  and  
 92  $\beta$  are growth and death or differentiation rate for intermediate cells respectively. This model can be  
 93 thought of as the initiation-promotion-progression paradigm of carcinogenesis.

## 94        **2.2. Non exposed tissue**

95            **2.2.1. Tissue description** Because deterministic models are not well suited to simulate  
96 heterogeneous tissue and as our lab is establishing a long-term computer framework for more complex  
97 radiation simulations, we use instead automata to simulate cancer incidence via the principle of TSCE.  
98 An important reason for this choice is the fact that it is easy to add new rules or different geometrical  
99 configurations in automata, making them an ideal framework for evolving simulations.

100 Simulations were performed using Matlab software (The MathWorks, Natick, MA, USA) and the  
101 advanced imaging platform DIPimage (Image Processing Toolbox for Matlab, Delft University of  
102 Technology, Delft, The Netherlands). The simulated tissue consists of an array of 100 X 100 pixels, with  
103 each pixel labeled with a particular stage. Fig 1A depicts conceptually the progression of a normal cell via  
104 successive mutations towards becoming a tumor cell, highlighting the importance of tissue proliferation  
105 for cancer to occur. The automata implementation of this progression is depicted in Fig. 1B with a flow  
106 chart showing decision algorithms. Stage 1 represents a normal cell (green pixel), Stage 2 (labeled in  
107 blue) is a cell harboring a potentially dangerous mutation in the context of cancer induction (i.e.  
108 initiated) and Stage 3 (red pixel) is a cell harboring the two necessary mutations to expand into a full-  
109 blown cancer. Fig. 1C shows snapshots of one simulation where tissue is progressing towards cancer  
110 over many years.

111 With the TSCE assumption, cell death is a necessary condition for neighboring cells to be dividing and  
112 potentially acquiring mutations. The automata approach assumes additionally that the tissue is in  
113 homeostasis which means that dead cells are rapidly replaced by newly dividing cells. Consequently,  
114 division and death rate are identical ( $\alpha=\beta$ ). It can be noted in Fig. 1B that all cells touching a dying cell  
115 are eligible to fill the gap that is left behind. The selection of which neighboring cell will fill the gap is  
116 drawn randomly. Thus, whenever a cell divides, the new cell filling this gap has an opportunity to

117 acquire a mutation related to carcinogenesis. In a general implementation of this model, if the mother  
118 cell carries  $n$  mutations, there is a probability that the daughter cell will carry  $n+1$  mutations. A cell  
119 harboring a lot of mutations is likely to be more unstable genetically. Because there is no clear law  
120 defining the relationship between progression and genomic instability, for now we are imposing a  
121 mutation rate proportional to the cell stage. This assumption allows us to reduce the number of  
122 mutation parameter to only one value: i.e.  $\mu$ , the spontaneous mutation rate in a healthy cell. Note that  
123 both stage 2 and 3 can be reached via various unique combinations of genes being mutated, but details  
124 on genetic changes that lead to this pre-cancer states are not necessary in this model, as it is fully  
125 encompassed by determining  $\mu$ . Mutation model can be summarized as:

$$126 \quad \mu_n = n \cdot \mu. \quad (5)$$

127 In this approach, division is therefore driven by the turnover of the tissue being simulated. In the case of  
128 breast, it has been shown that the cell death rate  $\beta$  is periodic due to the menstrual cycle of estrogen  
129 and progesterone. Rising progesterone levels drive mammary cells in ducts and alveoli to multiply for  
130 possible pregnancy. If not pregnant, progesterone levels drop and induce cell death of newly formed  
131 tissue. If we assume a 28-day cycle with an apoptotic peak between days 28 and 0, the death rate  
132 pattern for different ages can be modeled (Fig. 2A). The amplitude and average values used here are  
133 derived from the literature and they are lower with increasing age (14-16) with a rate  $\beta$  in the order of  
134  $10^{-3}$ /day/cell. At menopause, the death rate is considered flat and lower than the pre-menopause value  
135 (17). For each simulated person, the age at menopause for an *in silico* individual is established based on  
136 a triple Gaussian distribution (centers: 50.3 y.o., 42.9 y.o and 35.3 y.o.) as previously suggested (18)  
137 leading to a smooth drop of cell death in simulations as one can visualize in Fig. 2B. Note that  
138 parameters for normal cell turnover in the breast are not changed for the rest of this model since they  
139 are directly derived from the literature.



140           **2.2.2. Senescence** Senescent cells are also considered in this model. They are represented as  
141 pixels that are unable to divide nor die (i.e. Stage -1). In other words, senescent pixels no longer divide  
142 and have acquired resistance to apoptotic signals. Our senescence model takes into account the age of  
143 the tissue being simulated. Telomere-initiated cellular senescence is also included in the model by  
144 generating senescence in only dividing cells. Briefly, at each time step, a random number is generated  
145 for each stage 1 and stage 2 pixel. This number is compared to the senescence probability which  
146 changes as the square of the age of the tissue (19):

$$147 \quad p_{senescence} = sen_{factor} * age^2. \quad (6)$$

148 If the random number is less than  $P_{senescence}$ , the cell is set to stage -1. Running a parameter sweep on the  
149 senescence factor  $sen_{factor}$ , a value of  $5 \times 10^{-9}$ /day led to a curve matching the literature for primates (19)  
150 (Fig 2C). In addition, a baseline of 2% senescence was imposed on the tissue at the starting age of 20  
151 y.o. to reflect the primate data. Note that compared to primates, the age scale has been expanded to  
152 reflect the human life span. We also assumed that stage 3 pixels (cancer cells) cannot senesce anymore  
153 since they have acquired mutations that allow them to avoid telomere-dependent and oncogene-  
154 dependent senescence (20).

155           **2.2.3. Parameter calibration to match breast cancer data** Key parameters in the  
156 TSCE model are the mutation rates: i.e. initiation (with probability  $\mu_1=\mu$ ) and transformation ( $\mu_2=2\mu$ ).  
157 Because of our assumption about increase of genomic instability with progression, we only need to  
158 determine  $\mu$ . It turns out that cancer incidence frequencies are not only dependent on  $\mu$  but also on the  
159 size of the tissue being simulated. In order to understand this relationship, we performed a parameter  
160 sweep on  $\mu$  for different number of cells considered in each modeled duct, and determined values of  $\mu$   
161 that led to simulations matching published spontaneous cancer incidence. Note that Age-Specific SEER  
162 Breast Cancer Incidence Rates were taken from SEER cancer registry records 2008-2012  
163 ([http://seer.cancer.gov/csr/1975\\_2012/](http://seer.cancer.gov/csr/1975_2012/)) (21). Fig. 2D shows simulated cumulated cancer incidence  
164 predicted by the model for various initial tissue size being considered against SEER records (diamonds  
165 and dash-line for fit). Simulations were repeated 10 times with group of 50 *in silico* people and  
166 parameter sweep on  $\mu$  was conducted to lead to the lowest mean square error between prediction and  
167 published data. We show that simulations fit very accurately epidemiologic data for various tissue size  
168 as long as the mutation rate is adjusted consequently, noting that the larger the number of cells being  
169 simulated in the tissue, the lower  $\mu$  needs to be. This relationship was well behaved with a power  
170 dependence of  $\mu$  over the number cells being simulated ( $R^2>0.999$ , data now shown). Ideally, one would  
171 like to simulate tissue of realistic sizes, however this would be extremely time consuming for simulations  
172 and our data suggest as long as  $\mu$  is set accordingly with the tissue size, the model behaves correctly. We  
173 therefore used going forward for our radiation prediction an initial tissue size of 100x100, leading to a  $\mu$   
174 value of  $3.8 \times 10^{-6}$ . Each individual was simulated as a branch of a mammary duct made of 10,000 cells  
175 (22).

176 Parameters having the greatest impact on the final curve are  $\mu$  and  $\beta$ . Cell death rate  $\beta$  is defined by the  
177 menstrual cycle for normal cells only (stage 1), which represents the majority of the cells at the  
178 beginning of simulation (age 20) and is fixed by experimental data (Fig. 2A). On the other hand, once a

179 cell has become mutated, it becomes hormonal independent and cell death is only driven by genetic  
180 instability which increases with progression (see Fig. 1A). For example, high grade tumors have higher  
181 level of apoptosis and genomic instability which is usually correlated with poor prognosis (23-25). A  
182 parameter sweep was performed on the  $\beta$  value for stage 2 and stage 3 to best fit experimental  
183 incidence and values are summarized in Table 1, confirming  $\beta$  needs to increase with progression to get  
184 accurate cancer prediction.

185 Note that during parameter sweep, increasing either  $\mu$  or  $\beta_2$  and  $\beta_3$  led to higher cancer incidence and  
186 thus multiple solutions for the same final cumulated incidence at age 80. However, a single solution was  
187 obtained by minimizing the error along the full age dependence between the published data and the  
188 simulations. This was done by finely tuning  $\beta_2$  and  $\beta_3$  down while increasing  $\mu$ . Note that a cancer  
189 growth factor is also present in the model and was based on the assumption that it takes 20 years  
190 between an initiating event and a detectable cancer. The growth factor is a metric representing the  
191 ability of neoplastic cells (stage 3) to grow and expand over neighboring healthy cells. After a set  
192 number of iterations, all stage 3 cells take over their immediate neighbors. This process reflects the loss  
193 of contact inhibition in cancer cells and loss of checkpoints regulating mitosis. The tumor growth  
194 parameter was set to once a year for breast cancer and is easily tunable to model other types of more  
195 aggressive cancers and is relatively arbitrary since a cancer is scored in our model once 5% of the tissue  
196 has become stage 3.

197           **2.2.4. Impact of senescence on cancer incidence** We investigated the hypothesis that  
198 senescent cells can slow down cancer progression. The senescence response is widely recognized as a  
199 potent tumor suppressive mechanism (26-28). The senescent factor parameter was thus increased to  
200 reach various level of senescence at age 80 and the impact on cancer incidence was assessed. Our  
201 baseline level of senescence that was kept for the rest of the simulations gives around 13% senescence  
202 in the whole tissue and  $11.2 \pm 1.31$  % incidence at age 80. Increasing the final level of senescence to 40%  
203 only reduces the incidence of breast cancer to  $9.4 \pm 1.27$  %. The effect is more noticeable when  
204 senescence hits unrealistic values of 70% and above, leading to breast cancer incidence below 6%.

### 205 **3. Results**

#### 206 **3.1. Targeted effects**

207 After calibrating parameters to fit spontaneous cancer incidence from epidemiological data, our model  
208 was then used to predict level of excess breast cancer one would expect from exposure to low-LET. This  
209 was done by modifying transiently mutation and cell death rates using published data in human cells  
210 exposed to low-LET.

211 The additional death rate from radiation was derived from clonogenic data of Lin *et al.* who studied the  
212 response of nonmalignant MCF10A mammary epithelial cells (29) and dose dependence was simulated  
213 by using the alpha/beta fit model (see Table 2). However, cells are not expected to die readily after X-ray  
214 exposure, as this is not what is observed in cell culture and even less *in vivo*. Rather the cells undergo a  
215 few cell cycles before dying either through apoptosis, necrosis or mitotic catastrophe. Mitotic  
216 catastrophe is not a cell death mechanism *per se*, but the process by which the cell will lose its  
217 reproductive capacity: i.e. following exposure to radiation, some cell lines and cancer cell lines in  
218 particular will continue to divide despite harboring DNA damage. These uncontrolled divisions lead to  
219 the loss of chromosome material, up to the point that daughter cells are no longer able to divide. The

220 time it takes for a cell to die was therefore modeled in two ways. First, we assume that death was  
221 spread evenly through a 14-day period based on previous work (30). For example, implementation of  
222 this model led to an additional 5.7% of all cells being deleted randomly every day for 14 days following 3  
223 Gy X-rays (Fig. 3A – “beta const” model) before returning to the normal  $\beta$  value of Fig. 2A. The other  
224 death model we used assumed death rates change over time post-exposure with an exponential  
225 attenuation as suggested by *in vitro* work (31, 32). This was implemented by assuming an exponential  
226 decay over 14 days, imposing the same overall amount of death during the 14 day period following  
227 exposure. We tested two conditions: either 2 or 3 fold increased death at day 0 compared to the “beta  
228 const” model (i.e. “beta X2” model has 11% excess death at day 0 and “beta X3” model has 17% excess  
229 death at day 0 for 3 Gy exposure). Fig 3B illustrates the exponential model for “beta X3”.

230 In the two stage clonal expansion model (TSCE), mutation rates encompass many possible genetic  
231 targets to obtain an initiated ( $\mu_1$ ) or transformed ( $\mu_2$ ) cell. To predict the impact of radiation  
232 perturbation on the TSCE we now need to propose a model affecting the mutation rate after exposure  
233 to ionizing radiation. We will assume radiation induces a transient increase of  $\mu$  which is proportional to  
234 dose for 24 hours post-exposure. Let us explain why in the next paragraph.

235 As we and others have previously shown in great length, mutation rates are a function of radiation dose  
236 with larger genes being more likely mutated (33-35). In addition, gene location in the nucleus probably  
237 plays a role in mutation frequency since damage production and DNA repair are modulated by  
238 chromatin territories (36, 37) and therefore individual genetic predisposition are at play here. However,  
239 as a first gross approximation, one can argue that initiation and transformation mutation rates are  
240 mainly the result of point mutations or small deletions of a large and unknown DNA target and that  
241 large deletions induced by two separate DNA double strand breaks can be neglected since they often  
242 lead to cell death due to deletion of vital genes (35). This simplifies greatly the model by not requiring a

243 quadratic dose term and by assuming mutation rate is increased linearly with dose during exposure. The  
244 amplitude of such increase can be approximated using experimental data measuring DNA double strand  
245 break (DSB) levels in human cells. According to our previous work and literature data, baseline damage  
246 in peripheral blood lymphocytes (PBL) range from 0.004 foci/cell in children up to 0.2-1 foci/cell in  
247 healthy adult donors when measured either using the  $\gamma$ -H2AX assay or 53BP1 assay (38-41). Let us chose  
248 the mid-range value (0.5 foci/cell) as a baseline damage level without radiation in a healthy population.  
249 Thus, this level of endogenous damage is directly correlated to the spontaneous mutation rate  $\mu$ . Next,  
250 low linear energy transfer (LET) exposure yields approximately 30 DSB/cell/Gy (42). This gives a 30/0.5 =  
251 60 ratio for foci levels between control cells and cells irradiated by 1 Gy. This dose dependence can be  
252 generalized as followed in the TSCE model:

$$253 \quad \mu(D) = 60 \cdot \mu_n \cdot D \quad (7)$$

254 where  $D$  is in Gy and  $\mu_n$  is increased only for 24 hour post-exposure. Such perturbation is depicted in Fig  
255 3C for various doses.

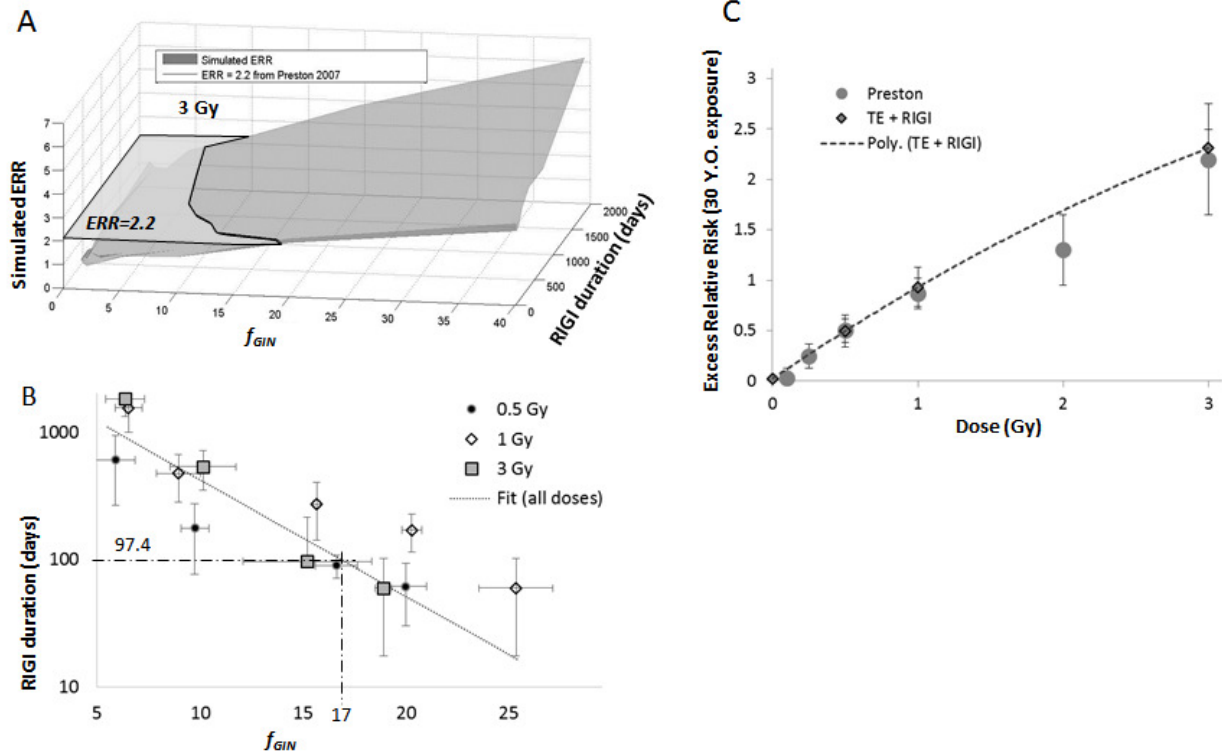
256 Radiation perturbations of  $\mu$  and  $\beta$  parameters in the TSCE model were simulated for doses of X-rays  
257 ranging from 0.05 to 3 Gy. Note that targeted effects were entirely modeled from experimental *in vitro*  
258 data and they were integrated into the TSCE model, making our simulations true predictions and not  
259 fits. The predicted excess relative risk (ERR) was compared to breast cancer ERR in atomic bomb  
260 survivors (4). Preston *et al.* computed ERR at age 70 for individuals irradiated at age 30 following  
261 Hiroshima and Nagasaki bombardments. Our simulations were therefore stopped at age 70 to match  
262 Preston reference, and the three different death models were tested (death rate constant – “beta  
263 const”, death rate decreasing exponentially – “beta 2X” and “beta 3X”). Simulations were carried out for  
264 10 groups of 50 people. Predicted ERR shown in Fig. 3D indicate that the exponential cell death rate  
265 models predict accurately the A-bomb data for large doses (2 and 3 Gy). This is not true for lower doses,

266 where predictions are well below the observed ERR. In contrast, constant cell death model leads to  
267 underestimation of the reported atomic bomb data for any simulated doses, which suggests that  
268 additional mechanisms have to be taken into account to explain the observed levels of cancer. We  
269 hypothesize in this case non-targeted effects are at play, which are investigated next.

### 270 **3.2. Non-targeted effects**

271 Non-targeted effects (NTE) reflect the impact of radiation on modifying cell signaling and the tissue  
272 microenvironment following exposure to ionizing radiation which lead to systemic changes in entire  
273 organs. These have additional impacts from the classic targeted effects (i.e. direct DNA damage and cell  
274 death already simulated in the previous section). We use modeling in this section to evaluate the level of  
275 NTE required to explain the lower cancer incidence we predicted in the low dose range by only  
276 considering targeted effects (Fig 3C).

277 Two NTE models were tested: radiation induced genomic instability (RIGI) and radiation-induced chronic  
278 inflammation (RICI). RIGI was implemented by increasing the mutation rate in the entire tissue in a  
279 uniform manner for prolonged periods after irradiation (i.e.  $\mu_{GIN} = \mu \cdot f_{GIN}$ ) where  $\mu_{GIN}$  is the new mutation  
280 rates in tissue when RIGI is active and  $f_{GIN}$  is the multiplicative factor induced by radiation. Let us use our  
281 model to evaluate  $f_{GIN}$  and see how it depends on dose. This can be done by doing a parameter sweep  
282 for RIGI duration and  $f_{GIN}$  leading to an array of simulated ERR. This is visualized in Fig. 4A, where  
283 predicted ERR for 3 Gy irradiation are shown as a plane. Irradiation was delivered *in silico* at age 30 and  
284 ERR assessed at age 70 to match the conditions used in the cancer breast A-bomb data (4). The  
285 intersection of the plane in Fig. 4A with the published ERR value (i.e. 2.2 at 3 Gy) represents all pair of  
286 duration and multiplicative factor  $f_{GIN}$  that can lead to the right ERR.



287  
 288 Fig 4B shows the resulting iso-ERR curves generated this way for three doses: 0.5, 1 and 3 Gy. One can  
 289 note that RIGI duration decreases exponentially with the multiplicative factor  $f_{GIN}$  for all three doses  
 290 simulated. The iso-ERR curves for all three doses are closest when  $f_{GIN} \sim 17$  and RIGI duration is  $\sim 97$  days  
 291 (dashed lines in Fig. 4B). Using these parameters, a new set of simulations predicting Preston ERR can be  
 292 computed (TE+RIGI scenario - Fig. 4C) clearly showing accurate predictions all the way down to 0.2 Gy.  
 293 Therefore our model confirms that RIGI is dose independent and is triggered by low level ionizing  
 294 radiation. Note that if we use instead the exponential cell death models (beta X2, beta X3), one cannot  
 295 find a set of values that can predict the ERR for all doses mainly because it always leads to overestimate  
 296 for doses larger than 1 Gy (data not shown).

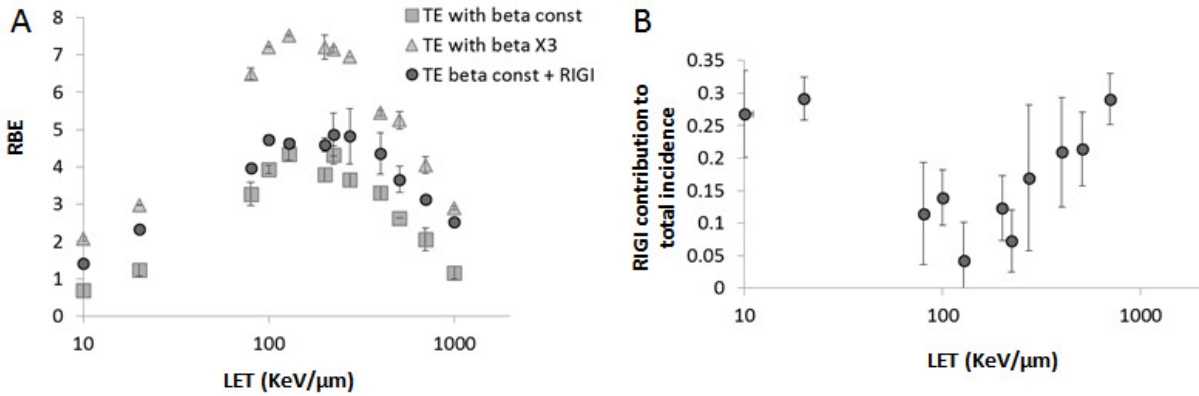
297 RICI was implemented by increasing the death rate in the entire tissue by a fold increase in a uniform  
 298 manner for prolonged periods after irradiation. The same approach that was applied for RIGI was done  
 299 for chronic inflammation (data not shown). Duration of 1825 days and induction fold of 2 were chosen  
 300 as the best fit. We noted however that The TE + RICI scenario gives less stable results than the TE + RIGI



301 scenario. This is mainly because there is one more step involved if the chronic inflammation is chosen as  
302 non-targeted effect. Indeed, cell mortality is tuned at a higher value, which implies more cell division to  
303 fill the gap left by the dead cell. Consequently it also implies more possibility for mutations, not because  
304  $\mu$  is higher but because there are more daughter cells that can be targeted. In the case of RIGI, only one  
305 process is at play: the mutation rate increases, the death rate and the number of targeted cells remain  
306 stable. In order to keep less variable outcome in our stochastic model, we chose RIGI as our principal  
307 non targeted effect in the rest of this work, allowing to keep the number of simulations reasonable to  
308 reach statistical significance.

### 309 **3.3. Modeling exposure to cosmic radiation**

310 For high LET exposure, the mutation and death rate from Fig. 3 were adjusted to reflect the change of  
311 radiation quality using published RBE. The change in death rate was made on the basis of our previous  
312 model predicting RBE for 10% survival in MCF10A cells exposed to high LET particles using the principle  
313 of DSB clustering as the main factor for higher cell death incidence than for low-LET (7). Even though  
314 MCF10A cells are immortalized, they are nonmalignant and they show similar response to primary  
315 human breast cells. For example, 10% cell survival of MCF10A is observed after 4 Gy (29) against 4.7 Gy  
316 for primary breast cells (43). RBE for mutation rate were based on a study that assessed HPRT<sup>-</sup> mutants  
317 in mammalian cells after exposure to a range of high LET particles (44). For non-targeted effect, the RIGI  
318 scenario was adopted and a RBE of 1 was used as we showed no dose dependence for RIGI in the  
319 previous section for low LET. This is in good agreement with our previous work showing in human breast  
320 cells that NTE are not increased with high-LET (43).



321 Fig 5A shows RBE prediction for breast cancer induction at age 70 after exposure to 1 Gy of high-LET  
 322 particles ranging from 10 to 1000 keV/μm with age of exposure at 30 y.o, the low-LET cancer incidence  
 323 dose dependence to compute the equivalent ERR (Fig 4C). The maximum RBE for breast cancer  
 324 induction peaks around 220 keV/μm with a value close to 5. For comparison, we used a mutational RBE  
 325 peaking at 100 keV/μm (44) while survival fraction RBE for breast cells peaks around 400 keV/μm using  
 326 our previous model (7). This illustrates the relative contribution of both mutational and death events,  
 327 leading to a competition between RBE peaks. For comparison, we also computed RBE when we only  
 328 have TE with the exponential cell death model (TE with beta X3) as this led to accurate low-LET ERR for  
 329 high doses only. As expected, this led to much higher RBE. Finally, in order to better characterize the  
 330 contribution of RIGI in RBE, we computed the scenario involving only targeted effects with beta  
 331 constant. One can note in Fig. 5A that the addition of RIGI at low and very high LET leads to a 2-fold  
 332 increase in RBE for breast cancer induction compared to TE alone (TE with beta const). Another way to  
 333 visualize the contribution of RIGI is to compute for each simulated LET the additional number of cancers  
 334 generated in the TE+RIGI scenario against TE only (using beta const in both case). This is shown in Fig. 5B  
 335 suggesting that nearly 30% of the excess cancers are due to RIGI at low and very high LET, while only  
 336 10% at intermediate LET. This is expected as RIGI is dose and LET independent, therefore when TE is  
 337 maximum (i.e. intermediate LET), RIGI has the lowest contribution. All radiation parameters are  
 338 summarized in Table 2.

340

## 341 **4. Discussion**

342 Modeling the complexity of the tissue response to ionizing radiation has been challenging because of  
343 the heterogeneity of tissue, the large time scale between exposure time and cancer detection, and the  
344 lack of experimental data needed to inform computer model. As such, deterministic models have been  
345 dominating the field (8, 10-13) with epidemiologic data from the A-bomb survivors remaining the gold  
346 standard for risk assessment (4). However, the growing complexity of data from radiation biology being  
347 unraveled over the past 20 years needs to be taken into account into outdated models and novel  
348 approaches bypassing the limitation of epidemiologic approaches have become a necessity for better  
349 risk management.

350 The old paradigm that biological consequences from exposure to radiation arise solely from events  
351 occurring at the time of exposure has been challenged in the last two decades by the observation of  
352 non-targeted effects (NTE) such as genomic instability, bystander and non-clonal effects, abscopal effect  
353 and delayed cell death (45, 46). All have in common that they are displaced in time or space from the  
354 initial insult and arise as a consequence of intercellular signaling. The argument has been made that  
355 irradiation is not only the initiating lesion but also promotes the acquisition of secondary genetic  
356 changes due to NTE, possibly involving long term tissue responses to radiation due to oxidative stress  
357 and cytokine production (47). In this work, we chose to concentrate on genomic instability and chronic  
358 inflammation for NTE, as they are readily applicable to the cell level used in our *in silico* tissue. Generally  
359 there is a lack of evidence for a conventional dose-response relationship for radiation-induced genomic  
360 instability (RIGI) with no increased expression at high doses and RIGI is modulated by cell type and  
361 genetic predisposition (48).

362 Persistent subclinical inflammation has been reported in Japanese A-bomb survivors (49). In a chronic  
363 inflammation context, production of reactive oxygen/nitrogen species by macrophages or neutrophils  
364 causes collateral damage in adjacent cells in the form of mutational events. It is thought that this  
365 chronic inflammation may confer predisposition to malignancies and has recently been linked to the  
366 development of radiation-induced leukemia (42). In addition, phagocytic uptake of apoptotic cells can  
367 result in further apoptosis by the release of soluble signals triggering Fas-mediated apoptosis in  
368 bystander cells (50). Another study correlated delayed apoptosis with the appearance of neoplastically  
369 transformed *foci* (51).

370 Over the years our group has developed approaches that distinguish themselves from the classic  
371 deterministic models. Our work has benefited from the usage of agent-based models (ABM), a  
372 stochastic approach simulating life and emerging properties of complex interacting entities (5, 7, 22).  
373 These modeling approaches are well suited for modeling NTE as they allow us to simulate and modify on  
374 the fly information related to spatial structure of a tissue, cell heterogeneity, large time scale and cell  
375 signaling. Our ABM models have already spanned from disruption of stem cell self-renewal signaling to  
376 three-dimensional breast epithelium reorganization and human breast senescence (6, 22). Others have  
377 also shown the efficiency of such approaches in modeling the radiation response (52, 53).

378 In the work presented here, we introduce a simplified agent-based model where a cell is a pixel which  
379 cannot move nor interact, but can die or divide to neighboring pixels. We refer to this model as an  
380 automaton. Removing the need for tracking individual agents allow us to gain computing speed and to  
381 lower memory usage for simulations. This was necessary to produce large *in-silico* cohorts of women  
382 exposed to a variety of radiation doses and radiation qualities in an attempt to predict cancer risk from  
383 exposure to cosmic radiation. We first implemented the two-stage clonal expansion (TSCE) model with  
384 automata to simulate tumor incidence arising spontaneously in human population due to random

385 mutations. As we have done in previous models (22), breast ducts cut along their length can be modeled  
386 as simple 2D sheet of one single cell layer. We also assume that initiated cells are still contact-inhibited  
387 and are still attached to the basement membrane and thus remain within the 2D sheet just like normal  
388 cells (6). On the other hand, proliferation potential and genomic instability is increased in initiated cells  
389 in our model. For TSCE, once an initiated cell acquires another set of gene mutations specific to  
390 transformation (mutation rate  $\mu_2$ ), it is classified as a neoplastic cell and its interaction with the  
391 basement membrane is compromised allowing it to proliferate inside the lumen (54). Lumen invasion  
392 has been modeled in sophisticated 3D *in silico* approaches (6, 55, 56) but these later models require  
393 large computer frameworks when handling millions of cells and millions of simulations. In order to keep  
394 size and simulation time manageable, we therefore kept the model as a 2D sheet where neoplastic cells  
395 invade neighboring cells instead of growing within the lumen in the case of 3D models. We found that  
396 detection time was a function of invasion parameters and detectable size programmed within the model  
397 and modifying these parameters only change the lag-time not the cancer frequencies. Therefore, using a  
398 3D model would not have changed our conclusions.

399 After identifying parameters leading to accurate spontaneous rate observed in the female population  
400 for breast cancer, we modeled an acute radiation exposure by modifying these parameters based on  
401 experimental data. We first modeled targeted effects (TE) by modifying mutation rates and cell death  
402 rates for a short duration after an acute exposure (1 and 14 days respectively). Perturbations of the TSCE  
403 model led to higher cancer incidence, allowing us to compute an excess relative risk (ERR) for various  
404 doses of low-LET. The predicted ERR were lower than A-bomb breast cancer ERR for doses lower than 2  
405 Gy, suggesting TE alone cannot fully explain radiation-induced carcinogenesis and that NTE are also  
406 contributing. The NTE model that best explained the A-bomb data was the induction of a chronic level of  
407 genomic instability  $\sim 17$  times higher than spontaneous levels lasting 97 days following exposure to low-  
408 LET. Induction of genomic instability was dose independent and thus added for all simulated doses

409 (>0.1Gy). On the other hand, the model could not let us conclude definitely on the absolute duration  
410 and intensity of radiation induced genomic instability (RIGI). For instance, a shorter duration could lead  
411 to the same outcome if genomic instability was set higher. To put this result into perspective let us  
412 compare the model to experimental observations. For in vitro data, it was shown that RIGI presents the  
413 same kind of mutation spectrum than spontaneous mutations and can persist over many cell doublings:  
414 i.e. more than 40 divisions in mammary epithelial cells exposed to  $\gamma$ -rays or neutrons (57). Similarly, *In*  
415 *vivo* experiments involving mice have reported RIGI lasting up to one year after irradiation (58).

416 Kaiser et al have also looked at the relative contribution of TE and NTE to fit the A-bomb ERR at 1 Gy  
417 using empirical models mixed with a deterministic implementation of TSCE (59). In their model, they  
418 concluded that the age dependence of ERR could be explained by three different modes of actions for  
419 radiation: either direct effect on initiation alone; long-life increase of proliferation of pre-cancerous  
420 cells; or long-life increase of genomic instability. In their model however, there are no biological  
421 parameters derived from experiments and the model does not represent spatial constraints from a  
422 tissue in homeostasis. In our case, we directly visualize the impact of various biological mechanisms on  
423 carcinogenesis, giving us more biological insights than simply fitting a curve.

424 Once the NTE model was established for low-LET, we challenged our model to predict breast cancer  
425 incidence in an artificial human cohort exposed to various high-LET particles. This was done by simply  
426 modifying the TE parameters using published RBE for cell death and mutation. In turn, we predicted RBE  
427 for breast cancer induction, which reached a maximum of 5 following 220 keV/ $\mu$ m. In contrast, RBE  
428 were close to 1 for LET>1000 keV/ $\mu$ m or LET<10 keV/ $\mu$ m. Note that the LET-dependence used for cell  
429 death RBE is based on the concept that DNA double strand breaks (DSB) are naturally gathered into  
430 common repair center (36, 60), a paradigm that leads to higher cell death at high dose or higher LET in  
431 human breast epithelial cells (7). One could have used published RBE on other cell lines (61) instead of

432 these theoretical RBEs. Using published RBE instead would still lead to similar cancer RBE since values  
433 and dose curve looked very similar. The advantage of using theoretical death RBE based on DSB  
434 clustering formalism (7) is the fact that we can predict any dose, dose rate and LET scenarii.

435 In order to put these RBE predictions into perspective, we should compare them to the most  
436 comprehensive dataset for tumor induction after high LET irradiation (2, 62). LET ranging from  $\sim 1.5$  to  
437  $170 \text{ keV}/\mu\text{m}$  were investigated in mice and RBE values for Harderian gland tumor incidence were  
438 measured to be much higher than our models with RBE  $\sim 27-40$  for  $^{56}\text{Fe}$ . The Harderian gland is not an  
439 organ present in humans, and these RBE discrepancies illustrate the ongoing challenge of scaling data  
440 from mice to humans. However, one potential explanation is the fact that NTE may account for some of  
441 these discrepancies reflecting the very distinct microenvironment of tissues and species. In particular,  
442 Cucinotta et al. derived an analytical model to fit the Harderian gland tumor prevalence and showed  
443 that NTE had a significant impact by increasing RBE for very low and very high LET (63). This result is in  
444 agreement with our model where NTE is triggered for any simulated doses in an equal manner, making  
445 it relatively more significant also at extreme LET or at low doses (Figs. 4C and 5).

## 446 **5. Conclusion**

447 At present, our automata model can provide RBE for breast cancer induction with a large panel of  
448 particle radiations. Other types of cancers can be implemented in a few steps. First, the calibration for  
449 spontaneous cancer induction has to be performed and spontaneous mutation and death rates will be  
450 obtained for a specific tissue. Next, the death rate following irradiation has to be adapted. This is easily  
451 done on the basis of survival fraction for a specific cell line exposed to X-rays and using our previous  
452 formalism on DSB clustering to predict death rate for high-LET radiation (7). However, a knowledge gap  
453 exists regarding RIGI with many remaining questions: Is there a dose threshold for RIGI? What is the

454 dependence of RIGI with respect to species and tissues? Is there any dose shape curve for RIGI past the  
 455 threshold? How does RIGI change in the context of chronic exposure?

456 Finally, in the context of space missions, in particular incoming missions to Mars where astronauts are  
 457 expected to be exposed to more than 1 Sv in the course of a three year mission, risks are currently  
 458 poorly determined. Space conditions of chronic low doses of high LET have been an ongoing challenge  
 459 for modeling long-term health hazard from space radiation. It may become a reality with our model, as it  
 460 provides a tool to simulate real space conditions with both LET and time scales being fully compatible  
 461 for chronic exposure over days or months. We believe in the future that physiological information  
 462 obtained on Astronauts before, during and after a mission could be integrated into our model to better  
 463 inform long-term effects such as NTE and RIGI and create more accurate risk models.

## 464 **Acknowledgments**

465 We wanted to thank Dr. Louise Viger for her constructive feedback on the manuscript. ACH is a  
 466 postdoctoral fellow supported by the Belgian American Education Foundation, the Fulbright Commission  
 467 and the Walloon region of Belgium (WBI). SVC, JT and AO are supported by NASA fundings  
 468 [NNL15AA08I].

469 **Table 1 Summary of Input parameters leading to accurate spontaneous breast cancer incidence.**

Input parameters	Value (day <sup>-1</sup> )
<i>Baseline</i>	
Death rate $\beta_1$ (stage 1 – hormonally driven) average at 20 y.o. (See Fig. 2A for all values)	1.8 e-3
Death rate $\beta_2$ (stage 2 – age independent)	3.1 e-3
Death rate $\beta_3$ (stage 3 – age independent)	5.6 e-3
Mutation rate $\mu_n$ (stage n $\rightarrow$ stage n+1)	n x 3.8 e-6
Senescence factor	5 e-9



Tumor growth

1/365

470

471 Table 2 Radiation parameters

<i>Targeted effects</i>	
<b>Low-LET</b>	
Radiation $\mu$ $\mu(D) = 60 \cdot \mu \cdot D$	Multiplicative factor proportional to dose
Radiation $\beta$ survival = $\exp(-0.084 \cdot D^2 - 0.273 \cdot D)$	Dose-dependent additive factor from clonogenic survival data from Lin et al. (29)
<b>High-LET</b>	RBE for $\mu$ (44) and for $\beta$ (7)
<i>Non targeted effects (LET and dose independent)</i>	
RIGI $\mu$	17 multiplicative factor
RIGI duration	97 days
Inflammation $\beta$	2 multiplicative factor
Inflammation duration	1825 days

472

## 473 References

- 474 1. Cucinotta FA, Durante M. Cancer risk from exposure to galactic cosmic rays: implications for  
475 space exploration by human beings. *The Lancet Oncology*. 2006;7(5):431-5.
- 476 2. Alpen EL, Powers-Risius P, Curtis SB, DeGuzman R. Tumorigenic potential of high-Z, high-LET  
477 charged-particle radiations. *Radiat Res*. 1993;136(3):382-91.
- 478 3. Chancellor JC, Scott GB, Sutton JP. Space Radiation: The Number One Risk to Astronaut Health  
479 beyond Low Earth Orbit. *Life (Basel)*. 2014;4(3):491-510.
- 480 4. Preston DL, Ron E, Tokuoka S, Funamoto S, Nishi N, Soda M, et al. Solid cancer incidence in  
481 atomic bomb survivors: 1958-1998. *Radiat Res*. 2007;168(1):1-64.
- 482 5. Mukhopadhyay R, Costes SV, Bazarro A, Hines WC, Barcellos-Hoff MH, Yaswen P. Promotion  
483 of variant human mammary epithelial cell outgrowth by ionizing radiation: an agent-based model  
484 supported by in vitro studies In Press. 2010.
- 485 6. Tang J, Enderling H, Becker-Weimann S, Pham C, Polyzos A, Chen CY, et al. Phenotypic transition  
486 maps of 3D breast acini obtained by imaging-guided agent-based modeling. *Integrative biology :*  
487 *quantitative biosciences from nano to macro*. 2011;3(4):408-21.
- 488 7. Vadhavkar N, Pham C, Georgescu W, Deschamps T, Heuskin AC, Tang J, et al. Combinatorial DNA  
489 Damage Pairing Model Based on X-Ray-Induced Foci Predicts the Dose and LET Dependence of Cell  
490 Death in Human Breast Cells. *Radiat Res*. 2014.
- 491 8. Ritter G, Wilson R, Pompei F, Burmistrov D. The multistage model of cancer development: some  
492 implications. *Toxicology and industrial health*. 2003;19(7-10):125-45.
- 493 9. Armitage P. Multistage models of carcinogenesis. *Environmental health perspectives*.  
494 1985;63:195-201.
- 495 10. Hayflick L. The Limited in Vitro Lifetime of Human Diploid Cell Strains. *Exp Cell Res*. 1965;37:614-  
496 36.
- 497 11. Pompei F, Polkanov M, Wilson R. Age distribution of cancer in mice: the incidence turnover at  
498 old age. *Toxicology and industrial health*. 2001;17(1):7-16.
- 499 12. Heidenreich WF, Luebeck EG, Hazelton WD, Paretzke HG, Moolgavkar SH. Multistage models  
500 and the incidence of cancer in the cohort of atomic bomb survivors. *Radiat Res*. 2002;158(5):607-14.
- 501 13. Heidenreich WF, Luebeck EG, Moolgavkar SH. Some properties of the hazard function of the  
502 two-mutation clonal expansion model. *Risk Anal*. 1997;17(3):391-9.
- 503 14. Anderson TJ, Ferguson DJ, Raab GM. Cell turnover in the "resting" human breast: influence of  
504 parity, contraceptive pill, age and laterality. *Br J Cancer*. 1982;46(3):376-82.
- 505 15. Potten CS, Watson RJ, Williams GT, Tickle S, Roberts SA, Harris M, et al. The effect of age and  
506 menstrual cycle upon proliferative activity of the normal human breast. *Br J Cancer*. 1988;58(2):163-70.
- 507 16. Navarrete MA, Maier CM, Falzoni R, Quadros LG, Lima GR, Baracat EC, et al. Assessment of the  
508 proliferative, apoptotic and cellular renovation indices of the human mammary epithelium during the  
509 follicular and luteal phases of the menstrual cycle. *Breast cancer research : BCR*. 2005;7(3):R306-13.
- 510 17. Li JJ, Li SA, Daling JR. *Hormonal Carcinogenesis III*: Springer Science & Business Media; 2001.
- 511 18. Greer W, Sandridge AL, Chehabeddine RS. The frequency distribution of age at natural  
512 menopause among Saudi Arabian women. *Maturitas*. 2003;46(4):263-72.
- 513 19. Herbig U, Ferreira M, Condel L, Carey D, Sedivy JM. Cellular senescence in aging primates.  
514 *Science*. 2006;311(5765):1257.
- 515 20. Campisi J, d'Adda di Fagagna F. Cellular senescence: when bad things happen to good cells.  
516 *Nature reviews Molecular cell biology*. 2007;8(9):729-40.
- 517 21. N H, AM N, M K, J G, D M, SF A, et al. SEER Cancer Statistics Review, 1975-2012, National Cancer  
518 Institute. Bethesda, MD. [http://seer.cancer.gov/csr/1975\\_2012/2015](http://seer.cancer.gov/csr/1975_2012/2015).

- 519 22. Tang J, Fernandez-Garcia I, Vijayakumar S, Martinez-Ruiz H, Illa-Bochaca I, Nguyen DH, et al.  
520 Irradiation of juvenile, but not adult, mammary gland increases stem cell self-renewal and estrogen  
521 receptor negative tumors. *Stem cells*. 2013.
- 522 23. Parton M, Dowsett M, Smith I. Studies of apoptosis in breast cancer. *Bmj*. 2001;322(7301):1528-  
523 32.
- 524 24. Gandhi A, Holland PA, Knox WF, Potten CS, Bundred NJ. Evidence of significant apoptosis in  
525 poorly differentiated ductal carcinoma in situ of the breast. *Br J Cancer*. 1998;78(6):788-94.
- 526 25. Zhao H, Morimoto T, Sasa M, Tanaka T, Izumi K. Immunohistochemical expression of uPA, PAI-1,  
527 cathepsin D and apoptotic cells in ductal carcinoma in situ of the breast. *Breast cancer*. 2002;9(2):118-  
528 26.
- 529 26. Campisi J. Aging, cellular senescence, and cancer. *Annual review of physiology*. 2013;75:685-  
530 705.
- 531 27. Rodier F, Campisi J. Four faces of cellular senescence. *J Cell Biol*. 2011;192(4):547-56.
- 532 28. Campisi J, Sedivy J. How does proliferative homeostasis change with age? What causes it and  
533 how does it contribute to aging? *The journals of gerontology Series A, Biological sciences and medical*  
534 *sciences*. 2009;64(2):164-6.
- 535 29. Lin YF, Nagasawa H, Peng Y, Chuang EY, Bedford JS. Comparison of several radiation effects in  
536 human MCF10A mammary epithelial cells cultured as 2D monolayers or 3D acinar structures in matrigel.  
537 *Radiat Res*. 2009;171(6):708-15.
- 538 30. Wera AC, Heuskin AC, Riquier H, Michiels C, Lucas S. Low-LET proton irradiation of A549 non-  
539 small cell lung adenocarcinoma cells: dose response and RBE determination. *Radiat Res*.  
540 2013;179(3):273-81.
- 541 31. Sakashita T, Hamada N, Kawaguchi I, Ouchi NB, Hara T, Kobayashi Y, et al. A framework for  
542 analysis of abortive colony size distributions using a model of branching processes in irradiated normal  
543 human fibroblasts. *PLoS One*. 2013;8(7):e70291.
- 544 32. Sakashita T, Hamada N, Kawaguchi I, Hara T, Kobayashi Y, Saito K. A branching process model for  
545 the analysis of abortive colony size distributions in carbon ion-irradiated normal human fibroblasts.  
546 *Journal of radiation research*. 2014;55(3):423-31.
- 547 33. Sachs RK, Brenner DJ, Chen AM, Hahnfeldt P, Hlatky LR. Intra-arm and interarm chromosome  
548 intrachanges: tools for probing the geometry and dynamics of chromatin. *Radiat Res*. 1997;148(4):330-  
549 40.
- 550 34. Wu H, Sachs RK, Yang TC. Radiation-induced total-deletion mutations in the human hprt gene: a  
551 biophysical model based on random walk interphase chromatin geometry. *Int J Radiat Biol*.  
552 1998;73(2):149-56.
- 553 35. Costes S, Sachs R, Hlatky L, Vannais D, Waldren C, Fouladi B. Large-mutation spectra induced at  
554 hemizygous loci by low-LET radiation: evidence for intrachromosomal proximity effects. *Radiat Res*.  
555 2001;156(5 Pt 1):545-57.
- 556 36. Costes SV, Ponomarev A, Chen JL, Nguyen D, Cucinotta FA, Barcellos-Hoff MH. Image-based  
557 modeling reveals dynamic redistribution of DNA damage into nuclear sub-domains. *PLoS Comput Biol*.  
558 2007;3(8):e155.
- 559 37. Chiolo I, Minoda A, Colmenares SU, Polyzos A, Costes SV, Karpen GH. Double-strand breaks in  
560 heterochromatin move outside of a dynamic HP1a domain to complete recombinational repair. *Cell*.  
561 2011;144(5):732-44.
- 562 38. Denoyer D, Lobachevsky P, Jackson P, Thompson M, Martin OA, Hicks RJ. Analysis of 177Lu-  
563 DOTA-octreotate therapy-induced DNA damage in peripheral blood lymphocytes of patients with  
564 neuroendocrine tumors. *J Nucl Med*. 2015;56(4):505-11.
- 565 39. Djuzenova CS, Elsner I, Katzer A, Worschech E, Distel LV, Flentje M, et al. Radiosensitivity in  
566 breast cancer assessed by the histone gamma-H2AX and 53BP1 foci. *Radiation oncology*. 2013;8:98.

567 40. Mumbrekar KD, Fernandes DJ, Goutham HV, Sharan K, Vadhira BM, Satyamoorthy K, et al.  
568 Influence of double-strand break repair on radiation therapy-induced acute skin reactions in breast  
569 cancer patients. *Int J Radiat Oncol Biol Phys.* 2014;88(3):671-6.

570 41. Tang j, Georgescu W, Deschamps T, Yannone SM, Costes SV. *Mathematical Modeling for DNA*  
571 *Repair, Carcinogenesis and Cancer Detection. Genomic Instability and Cancer Metastasis: Springer*  
572 *Science & Business Media; 2015. p. 75–93.*

573 42. Joiner M, Kogel Avd. *Basic clinical radiobiology.* 4th ed. London: Hodder Arnold ;; 2009. vi, 375 p.  
574 p.

575 43. Andarawewa KL, Costes SV, Fernandez-Garcia I, Chou WS, Ravani SA, Park H, et al. Lack of  
576 radiation dose or quality dependence of epithelial-to-mesenchymal transition (EMT) mediated by  
577 transforming growth factor beta. *Int J Radiat Oncol Biol Phys.* 2011;79(5):1523-31.

578 44. Kiefer J, Schmidt P, Koch S. Mutations in mammalian cells induced by heavy charged particles:  
579 an indicator for risk assessment in space. *Radiat Res.* 2001;156(5 Pt 2):607-11.

580 45. Lorimore SA, Coates PJ, Wright EG. Radiation-induced genomic instability and bystander effects:  
581 inter-related nontargeted effects of exposure to ionizing radiation. *Oncogene.* 2003;22(45):7058-69.

582 46. Wright EG, Coates PJ. Untargeted effects of ionizing radiation: implications for radiation  
583 pathology. *Mutat Res.* 2006;597(1-2):119-32.

584 47. Mukherjee D, Coates PJ, Lorimore SA, Wright EG. Responses to ionizing radiation mediated by  
585 inflammatory mechanisms. *The Journal of pathology.* 2014;232(3):289-99.

586 48. Wright EG. Inducible genomic instability: new insights into the biological effects of ionizing  
587 radiation. *Medicine, conflict, and survival.* 2000;16(1):117-30; discussion 31-3.

588 49. Neriishi K, Nakashima E, Delongchamp RR. Persistent subclinical inflammation among A-bomb  
589 survivors. *Int J Radiat Biol.* 2001;77(4):475-82.

590 50. Brown SB, Savill J. Phagocytosis triggers macrophage release of Fas ligand and induces apoptosis  
591 of bystander leukocytes. *Journal of immunology.* 1999;162(1):480-5.

592 51. Mendonca MS, Howard KL, Farrington DL, Desmond LA, Temples TM, Mayhugh BM, et al.  
593 Delayed apoptotic responses associated with radiation-induced neoplastic transformation of human  
594 hybrid cells. *Cancer Res.* 1999;59(16):3972-9.

595 52. Enderling H, Park D, Hlatky L, Hahnfeldt P. The Importance of Spatial Distribution of Stemness  
596 and Proliferation State in Determining Tumor Radioresponse. *Math Model Nat Pheno.* 2009;4(3):117-33.

597 53. Gao X, McDonald JT, Hlatky L, Enderling H. Acute and fractionated irradiation differentially  
598 modulate glioma stem cell division kinetics. *Cancer Res.* 2013;73(5):1481-90.

599 54. Bissell MJ, Rizki A, Mian IS. Tissue architecture: the ultimate regulator of breast epithelial  
600 function. *Current opinion in cell biology.* 2003;15(6):753-62.

601 55. Gatenby RA, Gillies RJ. Why do cancers have high aerobic glycolysis? *Nat Rev Cancer.*  
602 2004;4(11):891-9.

603 56. Macklin P, Edgerton ME, Thompson AM, Cristini V. Patient-calibrated agent-based modelling of  
604 ductal carcinoma in situ (DCIS): from microscopic measurements to macroscopic predictions of clinical  
605 progression. *J Theor Biol.* 2012;301:122-40.

606 57. Ponnaiya B, Cornforth MN, Ullrich RL. Induction of chromosomal instability in human mammary  
607 cells by neutrons and gamma rays. *Radiat Res.* 1997;147(3):288-94.

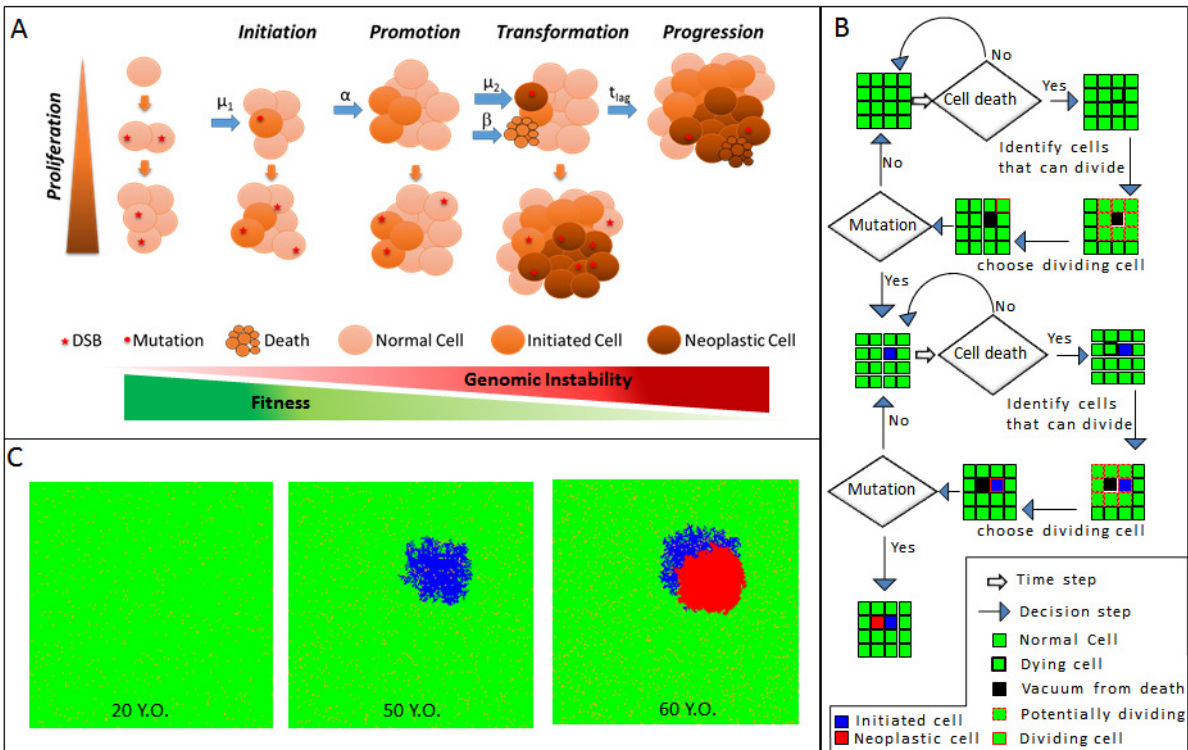
608 58. Watson GE, Lorimore SA, Wright EG. Long-term in vivo transmission of alpha-particle-induced  
609 chromosomal instability in murine haemopoietic cells. *Int J Radiat Biol.* 1996;69(2):175-82.

610 59. Kaiser JC, Jacob P, Meckbach R, Cullings HM. Breast cancer risk in atomic bomb survivors from  
611 multi-model inference with incidence data 1958-1998. *Radiation and environmental biophysics.*  
612 2012;51(1):1-14.

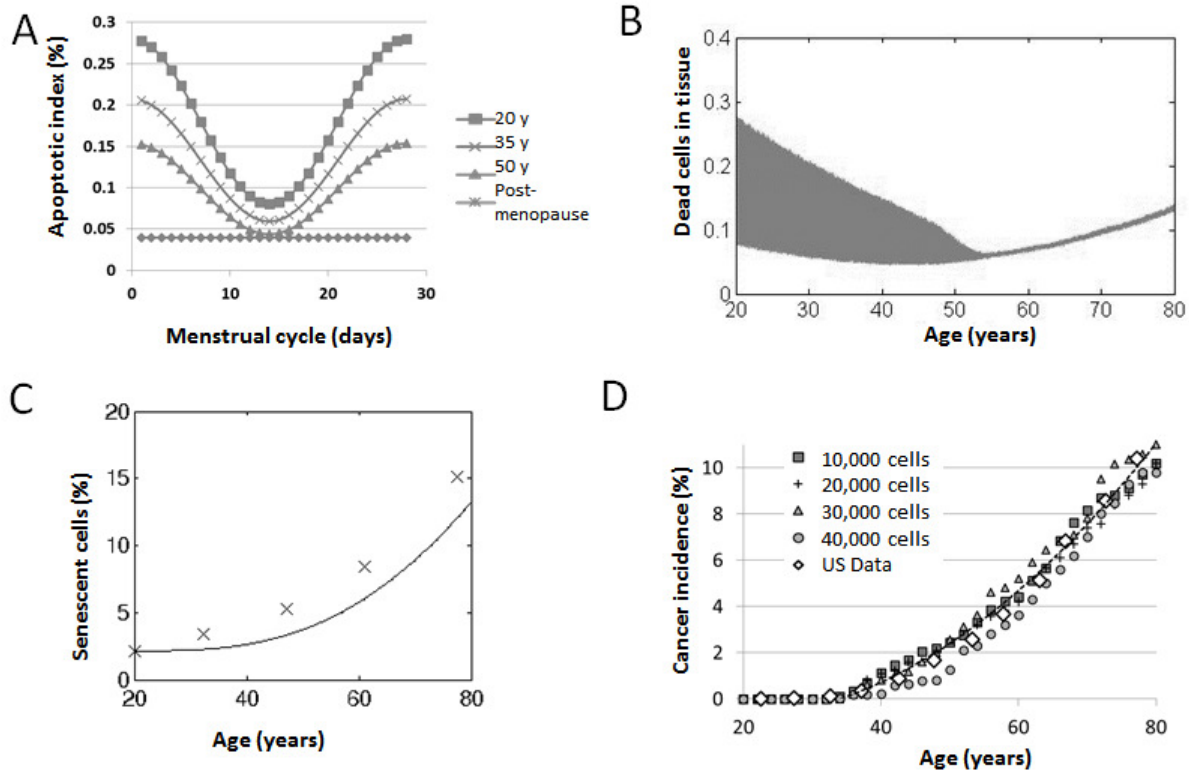
- 613 60. Neumaier T, Swenson J, Pham C, Polyzos A, Lo AT, Yang P, et al. Evidence for formation of DNA  
614 repair centers and dose-response nonlinearity in human cells. Proc Natl Acad Sci U S A. 2012;109(2):443-  
615 8.
- 616 61. Lett JT, Cox AB, Story MD, Ehmann UK, Blakely EA. Responses of synchronous L5178Y S/S cells to  
617 heavy ions and their significance for radiobiological theory. Proc R Soc Lond B Biol Sci.  
618 1989;237(1286):27-42.
- 619 62. Fry RJ, Powers-Risius P, Alpen EL, Ainsworth EJ, Ullrich RL. High-LET radiation carcinogenesis.  
620 Adv Space Res. 1983;3(8):241-8.
- 621 63. Cucinotta FA, Chappell LJ. Non-targeted effects and the dose response for heavy ion tumor  
622 induction. Mutat Res. 2010;687(1-2):49-53.

623

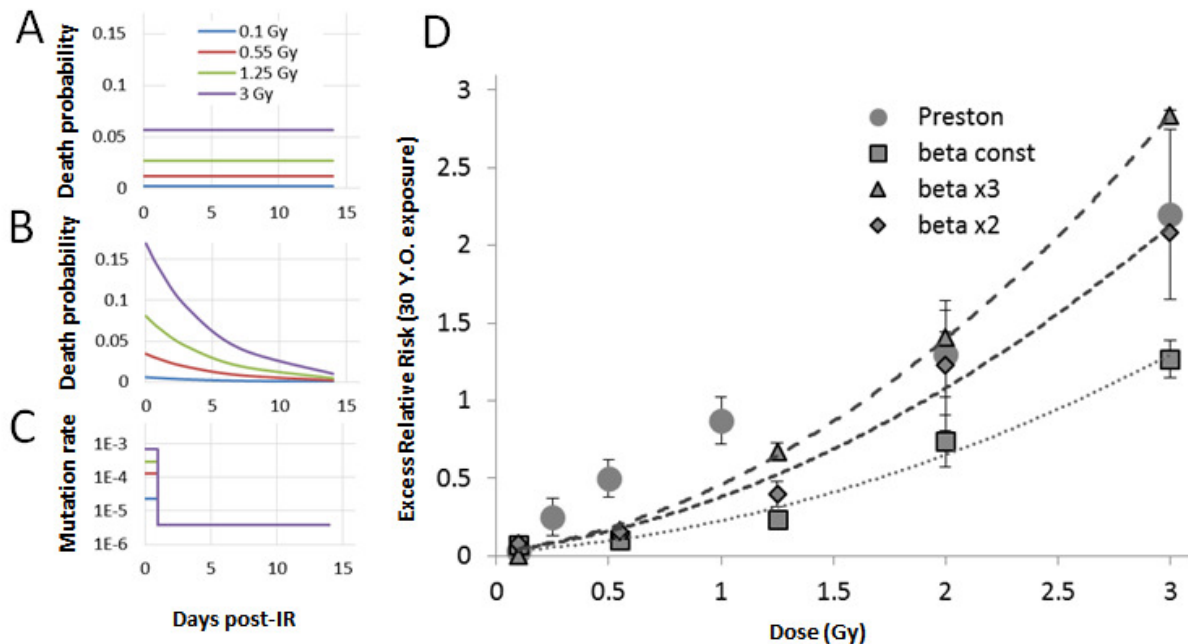
624 **Figure legends**



625  
 626 **Fig 1. Sketch of the automata carcinogenesis model.** (A) Illustration of TSCE, with  $\mu_1$  and  $\mu_2$  which  
 627 represent the mutation rates for initiated and malignant cells respectively.  $\alpha$  is the turnover rate  
 628 whereas  $\beta$  is the death rate.  $t_{iag}$  is the necessary time for a detectable tumor to form. (B) Flow chart of  
 629 automata illustrating how a pixel can become a tumor cell. (C) Snapshot of one simulation leading to a  
 630 tumor: (Green) Normal cell, (Blue) Initiated cell, (Red) Malignant cell, (Orange) Senescent cell.

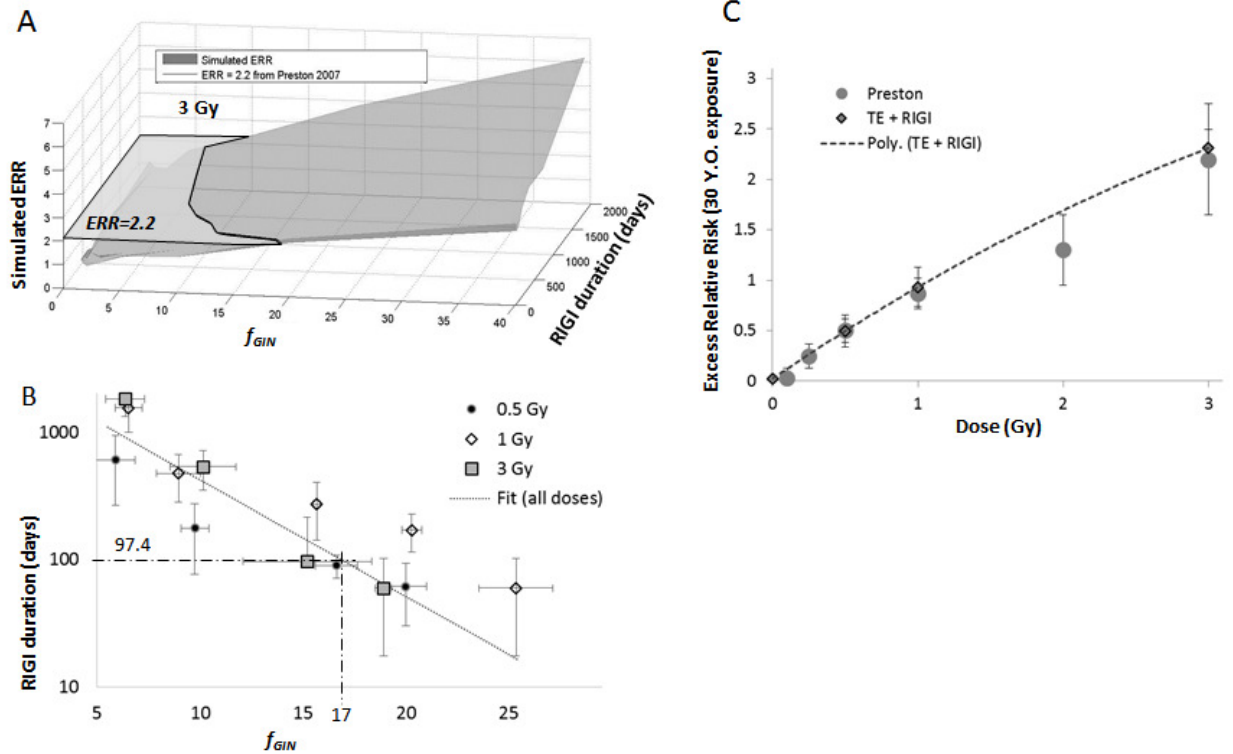


631  
632 **Fig 2. Model calibration on spontaneous breast cancer incidence.** (A) The death rate  $\beta$  is set periodic to  
633 match the menstrual cycle, with an amplitude and baseline that decreases with age until reaching  
634 menopause where rate stabilizes at  $0.4e-3$  per day. (B) Average number of dying cells as tissue ages *in*  
635 *silico*. (C) Simulation of the percentage of senescent cells in the tissue compared to published data for  
636 primate (19). Best fit is obtained for a senescence factor =  $5e-9$  and was set as a fixed parameter. (D)  
637 Average simulations of 500 tissues *in silico* predicting cumulated incidence of breast cancer at a given  
638 age (21). Calibration parameters that led to the lowest mean error square between predicted cancer  
639 incidence and epidemiological data for the US are given in Table 1. Calibration of mutation rate was  
640 done for various initial tissue sizes (i.e.  $100 \times 100$ ,  $200 \times 100$ ,  $200 \times 150$ ,  $200 \times 200$ ), showing large initial  
641 tissue leads to lower mutation rate.

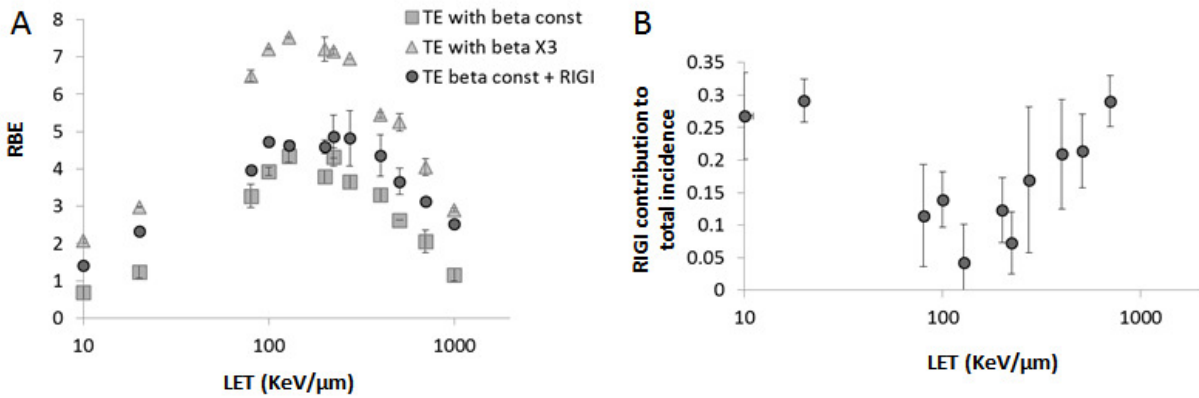


642  
 643 **Fig 3. Model calibration for low LET induced breast cancer incidence.** (A) Death levels are set based on  
 644 clonogenic data but with death spread evenly over a 14 day period (30). (B) Second death model,  
 645 assuming the same overall level of death but with death spread following an exponential decay over 14  
 646 day period (31, 32). In this example, initial death at day 0 is 3 times larger than in the constant model in  
 647 (A). We also considered 2 fold differences. (C) Mutation rates are assumed to be increased only for one  
 648 day after exposure to ionizing radiation. For simplification rate of mutation is set proportional to the  
 649 baseline rate found for spontaneous damage based on experimental data using a linear dependence  
 650 with dose (see Material and Method). Legend shows some of the tested doses in Gy. (D) Predicted  
 651 excess relative risk dose dependence of breast cancer at age 70 assuming exposure at age 30. Each solid  
 652 line represents a set of 500 simulated in silico women, exposed at a given age using TE only scenario.  
 653 Simulations for various cell death models are compared to A-bomb data (4) (plotted as full circles for age  
 654 of exposure equals to 30 y.o.).





655 **Fig 4. Simulated ERR at age 70 using TE + RIGI scenario as a function of mutation rate and duration. (A)**  
 656 Simulations for 3 Gy exposure at age 30. Experimental ERR (4) is shown intersecting predicted ERR,  
 657 allowing to define a set of mutation rate and duration that lead to accurate ERR. (B) RIGI duration and  
 658 mutation rates giving the right ERR for irradiation with 0.5, 1 or 3 Gy X-rays. Dashed line shows the point  
 659 couple chosen for subsequent simulations (induction fold of 17 over 97 days) (C) Predicted excess  
 660 relative risk dose dependence of breast cancer at age 70 assuming exposure at age 30 using TE+RIGI  
 661 scenario.



663  
 664 **Fig 5. Predicting high-LET RBE.** (A) RBE for breast cancer induction following irradiation with 1 Gy of  
 665 charged particles of various LET. (Circles) Targeted effect (beta const) + radiation induced genomic  
 666 instability scenario; (Squares) Targeted effect alone (beta const); (Triangles) Targeted effect alone using  
 667 exponential decay model for radiation-induced cell death (B) Fractional contribution of non-targeted  
 668 effects to breast cancer induction after irradiation with charged particles of various LET.

669  
 670  
 671  
 672